X-Ray Measurements of Mass Distributions in the Near-Nozzle Region of Sprays from Standard Multi-Hole Common-Rail Diesel Injection Systems

P. Leick[1*], A.L. Kastengren[2a], Z. Liu[2b], J. Wang[2b] and C.F. Powell[2a]
[1] Robert Bosch GmbH, Corporate Research, Gerlingen, Germany
[2a] Center for Transportation Research, Argonne National Laboratory, Argonne, USA
[2b] Advanced Photon Source, Argonne National Laboratory, Argonne, USA

Abstract

Unlike most quantitative optical measurement techniques, x-ray-radiography is not restricted by multiple scattering effects, and it has been demonstrated in recent years that the mass distribution in a Diesel spray can be deduced from the measured extinction of a monochromatic x-ray beam, even in the dense near-nozzle region. In prior applications of the technique, single- or three-hole research nozzles were generally used, and data evaluation was almost exclusively based on radiography measurements. In this paper, the first application involving standard, 5-hole production-type passenger car nozzles is reported, and the radiography results are complemented by a comprehensive set of high-quality optical spray images. The combination of the two techniques leads to a very thorough description of the sprays and is used to investigate the influence of gas density on the spray properties.

Introduction

The injection system of a modern Diesel engine plays an important role regarding the fuel/air mixture preparation, and hence on power, fuel consumption and emissions [1]. At the current high level of engine development, further improvements can only be based on a detailed understanding of all the processes involved in the atomization of the fuel jet and its subsequent evaporation and combustion. However, current models of the internal structure of high-pressure Diesel sprays are still speculative, reflecting the limited amount of available reliable experimental data [2]. Studies of fuel sprays typically rely on non-intrusive optical measurement techniques, but in the dense primary break-up region close to the nozzle outlet, the spray core is generally surrounded by a cloud of small droplets that is opaque to visible light. Information obtained from most optical measurement techniques is thus restricted to the spray periphery which, however, contains only a small fraction of the total fuel mass.

In the x-ray part of the electromagnetic spectrum, absorption replaces elastic scattering as the dominant interaction mechanism between fuel parcels and incoming photons. Since the attenuation of a monochromatic x-ray beam does not depend on the exact shape of the spray, but only on the total fuel mass contained within the beam path, x-ray radiography can be used to map the mass distribution in the spray, even in the dense near nozzle region. Several applications of this technique have been reported by Argonne National Laboratory (ANL) and collaborators, with spray characteristics such as local fuel density, droplet accumulation at the spray tip and different definitions of jet velocities being investigated [3-6].

Diesel spray research still relies heavily on knowledge gained from experiments where custom made nozzles with single axial holes are used and the fuel is injected into a gas at ambient atmospheric pressure. However, production-type multi-hole nozzles are characterized by a sharp bend in the fuel flow and by injections into extremely dense atmospheres. It is thus questionable whether the same break-up mechanisms are dominant in these different types of experiments. As it is still relatively straightforward to obtain the necessary unobstructed "optical" access to the spray under investigation using three-hole nozzles, and as they have a very similar layout to production-type nozzles (where 5-10 spray holes are typical), three-hole nozzles are often considered to be good substitutes for production-type nozzles, and have been used previously for measurements of the mass distribution in the spray [7]. Similar experiments with a higher number of spray holes are much more challenging. One possibility is to deflect neighboring sprays away from the field of view using nozzle caps [8]. This approach has been followed by Ramírez et al. for a heavy-duty injection system [9], but it could not be ruled out that there was an accumulation of minor fuel quantities from the unobserved spray plumes near the outlet of the spray hole under investigation.

[*]Corresponding author, philippe.leick@de.bosch.com

For the present study, a 5-hole passenger-car Common-Rail system was chosen as a starting point. In order to separate the effects of the aerodynamic forces from those of the other break-up mechanisms, two sets of experiments were performed, first at a high ambient density representative of actual engine conditions, and then under atmospheric conditions. Additionally, a 3-hole version of the same nozzle design was also used. Detailed optical images of the sprays were also recorded for all operating points, which provided valuable additional information about the spray structure and also made it possible to check the functionality of the spray cap used on the 5-hole nozzle.

Experimental Setup

The experiments described in this report were performed at the 1-BM-C beam line of the Advanced Photon Source (APS) at Argonne National Laboratory (ANL). The synchrotron radiation produced by the APS, a 7 GeV electron storage ring, first passes through a collimating mirror, then through a multilayer monochromator and a harmonic rejection mirror. This creates a narrow x-ray beam with a size of about 0.3×0.7 mm^2 and a narrow bandwidth ($\Delta E/E_v \sim 10^{-2}$) which is directed towards the experiment (Fig. 1).

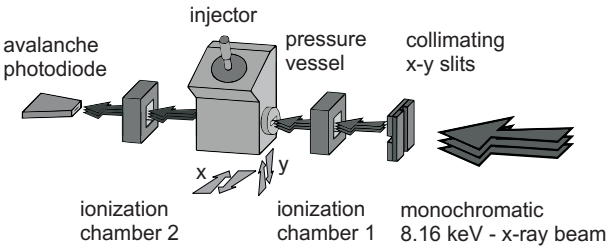

Figure 1: Schematic representation of the experimental setup. The pressure vessel is mounted on a computer-controlled *x*-*y*-translation stage.

Spatial resolution is limited by the size of the beam at the spray location. Therefore, before entering a pressure vessel with specially designed thin x-ray windows, the beam size is reduced to about 100 µm (FWHM, full width half maximum) in axial (x) and 15 µm FWHM in transverse (y) direction using a pair of vertical and horizontal slits. The total energy of each x-ray pulse transmitted through the spray chamber is measured by an Avalanche Photodiode and recorded with a digitizing oscilloscope. As a control, the time averaged beam power is continuously monitored by two ionization chambers.

The fuel is injected into the pressure vessel using a Bosch Common-Rail injector and fuel supply system capable of delivering rail pressures up to $p_I = 135$ MPa. The injector is oriented in such a way that the spray axis corresponds to the horizontal x-axis. The correct function of the injection system (see Table 1 for the relevant nozzle properties) and the nozzle cap was verified using an optical imaging system: for the 5-hole nozzle, fuel from the deflected sprays could not be found within the field of view at any time during the injection event; this was also the case for the three-hole nozzles, where it was not necessary to mount a cap.

Number of holes	Nozzle type	Orifice geometry	Outlet diameter	Height angle
5	mini-sac	ks 1.5	$D_O = 130$ µm	$\Psi = 75°$
3	mini-sac	ks 1.5	$D_O = 130$ µm	$\Psi = 75°$

Table 1: Geometric nozzle parameters (explained in detail in [10])

For the 5-hole nozzle, 20 mm^3 of fuel were injected at a rail pressure of $p_I = 80$ MPa, corresponding to an injection duration of ~1 ms. For the 3-hole nozzle, the energization pattern of the solenoid actuator was left unchanged, resulting in an almost identical injection duration, but a reduced fuel quantity of 15 mm^3. The spray chamber can be pressurized up to $p_G \leq 2.1$ MPa (absolute). When filled with nitrogen (N_2) at room temperature, the selected operating pressure of 1.85 MPa is equivalent to a gas density of $\rho_G = 21$ kg/m^3, a typical value at the moment of injection in a passenger car engine at high part-load-conditions. The low-pressure experiments were done at $p_G = 0.125$ MPa, corresponding to $\rho_G = 1.4$ kg/m^3. This value is slightly above atmospheric pressure, as a purge flow inside the chamber is necessary in order to minimize fog formation. Since the nozzles employed in this study are free of cavitation, changes in nozzle flow due to the decreased back pressure p_G are assumed to be negligible and all observed differences can be attributed entirely to the interaction of the liquid fuel with the surrounding atmosphere.

In order to increase its x-ray extinction coefficient, the fuel is doped with a cerium (Ce) additive. The x-ray absorption of materials is strongly dependent on kinetic photon energy, which is thus selected in order to optimize the absorption of fuel and additive compared to the extinction due to the chamber fill gas. At the photon energy ($E_v = 8.16$ keV) used in this study, the nitrogen is nevertheless responsible for a significant loss of incident x-ray

intensity, but this does not negatively affect the signal-to-noise ratio as the remaining photon flux is still more than sufficient.

Data Processing Methods

For monochromatic x-rays, the beam attenuation is described by the simple Beer-Lambert-law:

$$I(t) = I_0 \exp\left[-\int \mu_M \, \rho(z, t)\, dz\right] = I_0 \exp\left[-\mu_M \cdot M'(t)\right]. \quad (1)$$

In this equation, $I(t)$ and I_0 are the transmitted and incident beam intensities (i.e. during and before the injection), μ_M is the extinction coefficient (per mass/area) and ρ the *local* fuel density in the spray, which will generally be lower than the density ρ_F of the undisturbed liquid. $M' = \int \rho(z)\, dz$ is the projected mass per unit area along the beam path (z-axis). Since I_0 is constant during the injection, it is straightforward to calculate $M'(t)$ at different positions in the spray using (1). The normalization with I_0, which is determined individually for each injection, ensures that x-ray extinction *not* due to the fuel spray (i.e. nitrogen, chamber windows, fuel mist,…) does not induce any errors in the calculation of M'. It should be stressed that since radiography is a line-of-sight technique, the measured data points $M'(x, y)$ represent the projection of the actual, three-dimensional mass distribution on a two-dimensional plane perpendicular to the x-ray beam. Accordingly, M' is measured in units of mass/area [µg/mm^2].

During each injection, the attenuation is measured only for the small portion of the spray illuminated by the x-ray beam (coordinates: x, y). The spatial spray structure is examined by moving the spray chamber to many different positions along an optimized measurement grid, performing measurements at each point. Furthermore, the signal-to-noise ratio is improved by averaging the intensity traces for 32 or 64 different injections. Thus, the measurements represent the ensemble-averaged behavior of the spray.

Mass Distributions

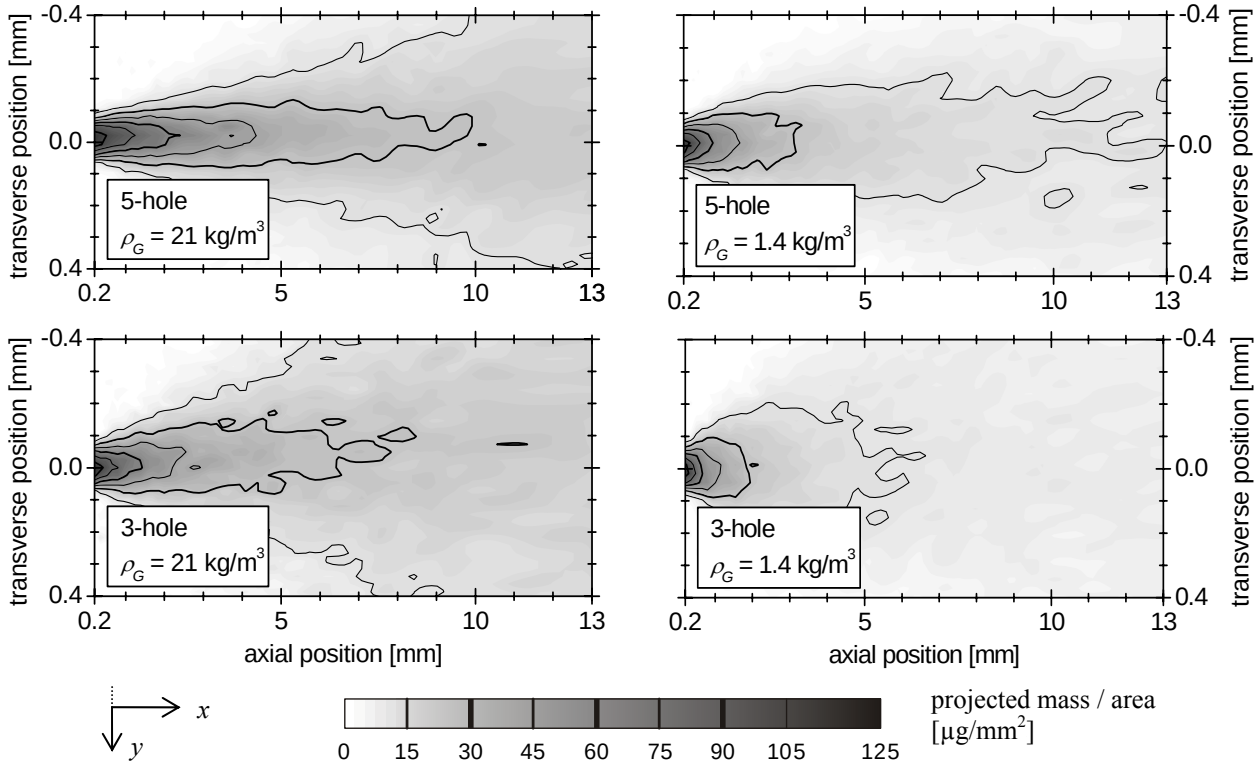

Figure 2: Projected mass/area [µg/mm^2] during the quasi-steady phase of the injection (t = 0.9 ms)

Figure 2 shows the mass distributions measured for the 5- and 3-hole nozzles at high and low ambient densities during the quasi-steady phase of the injection. The time t is given in relation to the start of energization of the solenoid coil. Fuel can first be seen leaving the nozzle at $t = 0.35$ ms, and once the spray tip has left the field of view ($t \sim 0.5$ ms, with slightly different values according to the operating conditions), there is almost no noticeable change in the mass distributions until the end of injection, which occurs around $t \approx 1.3$ ms.

The highest values of the local fuel concentration are found just after the nozzle outlet, and most of the fuel is located in a very narrow zone around the spray axis. There is a very rapid decrease of the projected fuel mass with increasing distance from the orifice. While the differences in the mass distributions from the 5- and 3-hole nozzles are relatively small, the influence of the ambient density is obvious. Comparing these results with previous investigations where measurements were carried out at different ambient densities [4, 5, 7, 11] suggests that, for strongly hydroground nozzles, spray shapes and mass distributions change significantly when the gas density is varied at low values (~ 1-6 kg/m^3), but that these changes are much less pronounced once the gas density is above ~ 10 kg/m^3.

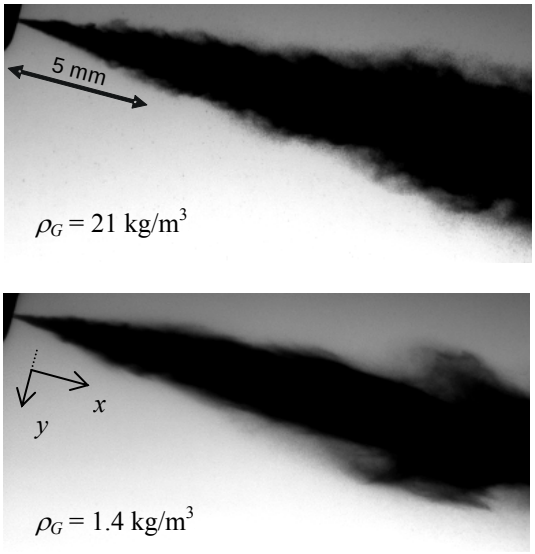

Figure 3: Shadow images of the sprays from the 3-hole nozzles, steady phase of the injection ($t = 0.9$ ms). The images have been selected to be representative of a much larger set of images recorded under identical conditions. A description of the test rig used to photograph these sprays can be found in [12].

It is interesting to compare the mass distributions with shadow images of the sprays (Figure 3). As expected, the "optical spray widths" are much higher than the corresponding widths derived from mass distributions, and the optical cone angles increase with ambient density. Unlike the x-ray data, which is ensemble averaged over a very large amount of distinct injections, the photographs are from individual injection events. Thus, it is not surprising to find some irregular features near the spray periphery. At high ambient density, these structures are rather small, as are the fluctuations between images taken from different injections. Large scale structures can be seen at low ambient density, and the fluctuations between different images are much more pronounced, giving the overall impression that the spray is less stable.

Spray Width

At different distances x from the nozzle outlet, the width of the spray can be determined. For the radiography data, the criterion is full width / half maximum of the projected mass distributions; more details about the calculation method can be found in [7]. The optical spray width is determined using statistics on a set of individual images recorded at the same time after the start of injection. Roughly, the criterion used defines the spray border as the locations where there is a 50%-probability of detecting liquid fuel (i.e. dark areas) in any given image; details can be found in [8]. Results of these evaluations, averaged during the quasi-steady phase of the injection, are shown in Figure 4.

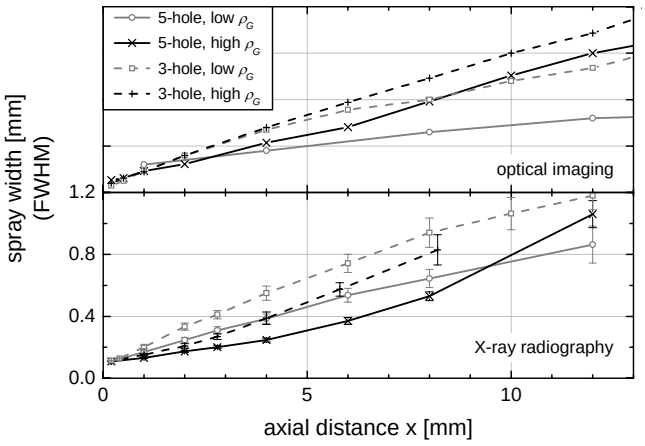

Figure 4: Average spray widths during the steady phase of the injection ($t = 0.9 \pm 0.2$ ms)

The evaluation clearly confirms that the values of the optical spray width are much higher than the values based on the mass distributions. Both techniques show that, at high and at low ambient density, the sprays from the 3-hole nozzles are wider than those from the 5-hole nozzle, despite the fact that the spray hole ge-

ometries are almost identical. The most plausible assumption is that these differences can be traced to changes in the nozzle sac flow; since all the sprays were carefully checked to be symmetric, spray asymmetry can be ruled out as an explanation. Based on the evaluation of the optical images, the spray widens with increasing ambient density as expected, although the influence of ρ_G seems lower than predicted by the literature, where the cone angles are often assumed to be proportional to $(\rho_G / \rho_F)^{1/2}$ [13]. The situation is different for the mass-based spray widths: close to the nozzle outlet, the widths are actually lower at high ambient density; further downstream ($x \gtrsim 10$ mm), however, the spray width is higher for the high ambient density cases. The mass-based spray width is *not* proportional to x: the corresponding curves seem to have different slopes in the near-nozzle and in the downstream spray regions. Interestingly, the near-nozzle slope is higher than the downstream slope under atmospheric conditions while the reverse is true at high ambient density.

Axial Mass Distribution and Spray Velocity

Additional information about the spray structure can be obtained by examining the axial mass distribution, which is shown in Fig. 5a.

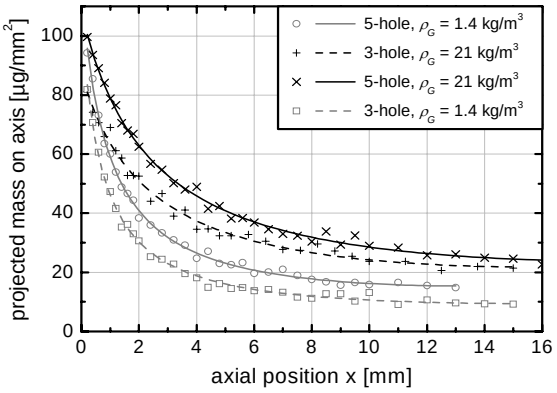

Figure 5a: Mass/area on the (dynamically defined) spray axis; the points correspond to the measured values, the lines represent fits to the data.

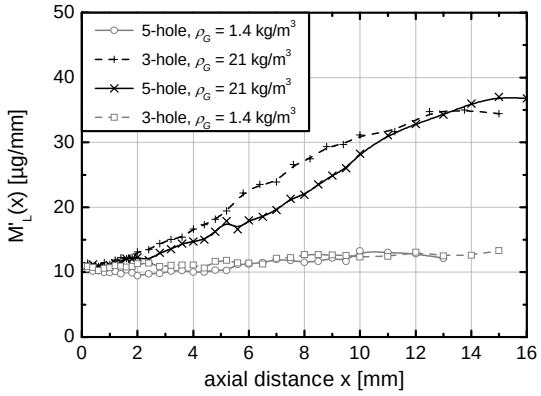

Figure 5b: Transverse integrated mass

The curves representing the projected mass along the spray axis confirm that, as already indicated by the projected mass distributions (Fig. 2), there is a rapid drop of the local fuel concentrations with increasing distance from the nozzle, and that this drop is faster under atmospheric conditions. Since the injection rate is identical for all the operating conditions, there should be less mass along the beam path for a wide spray than for a narrow spray. This is indeed the case when comparing the sprays from the 5- and 3-hole nozzles, but not so for the two different ambient densities. An explanation can be found by examining the transverse integrated mass $M'_L(x)$ (Fig. 5b), which is the total fuel mass detected at a given distance x from the nozzle outlet plane:

$$M'_L(x) = \int M'(x,y)\, dy \approx \sum_i M'(x,y_i)\, \delta y_i \tag{2}$$

For atmospheric conditions, the transverse integrated mass is nearly constant and independent of the number of spray holes during the quasi-steady phase of the injection. At high ambient density, a noticeable increase of the transverse integrated mass with downstream distance can be seen, which means that fuel accumulates along the jet path. The rise of M'_L with x seems to stop at distances of $x \gtrsim$ 12-15 mm. This is not a real effect, but can be explained by the small width of the x-ray windows. At high distances from the nozzle outlet, the spray has widened so much that its outer peripheral regions are no longer within the accessible field of view. Thus, the increase in M'_L stops sooner for the spray from the 3-hole nozzle, which is wider than the spray from the 5-hole nozzle.

The transverse integrated mass is closely related to the mean spray velocity [6]. For steady sprays, the mass flow through planes normal to the main spray direction is independent of the distance x to the nozzle outlet:

$$\iint v_x(x,y,z)\, \rho(x,y,z)\, dy\, dz = const \equiv \tilde{v}_x(x) \iint \rho(x,y,z)\, dy\, dz = \tilde{v}_x(x)\, M'_L(x) \tag{3}$$

In Eq. 3, $\widetilde{v}_x(x)$ is defined as the mass-averaged axial spray velocity. It should not be confused with the velocity of the spray tip, which will generally be lower, and for which the "steady spray" assumption cannot be valid. For a steady spray, $\widetilde{v}_x(x)$ is inversely proportional to $M'_L(x)$. The increased mass accumulation along the spray axis at high ambient density is thus a natural consequence of the loss of spray velocity due to aerodynamic drag. Since the spray from the 3-hole nozzle is wider than the one from the 5-hole nozzle, the leading spray regions are expected to be less effective at shielding the trailing droplets from aerodynamic resistance, and the slowdown of the spray is expected to be more rapid. This is confirmed by the results shown in Fig. 5b, where the increase of $M'_L(x)$ is seen to be more pronounced for the 3-hole nozzle. At atmospheric ambient conditions, only a very slight increase of $M'_L(x)$ can be seen, which indicates that the velocity losses in the spray are very small.

The analysis presented here is based on an idealization of the actual spray behavior, since its validity depends on the approximation of a perfectly steady spray. Nevertheless, the projected mass distributions do not change much during most of injection event, apart for the beginning and end of injection.

Summary

The experiments presented in this paper represent a further step towards the ambitious objective of performing x-ray radiography measurements of Diesel sprays under realistic engine conditions. For the first time, production-type passenger car nozzles were used; to obtain an unobstructed view of one of the spray plumes, special nozzle caps were developed. It was carefully checked via optical imaging that the sprays are symmetric and that the use of the cap does not disturb the observed spray. The comparison of production 5-hole nozzles with 3-hole research nozzles, where the cap is not needed, has shown that while the break-up mechanisms seem to be very similar, there still are some important differences in the spray structure. Additional control experiments conducted at atmospheric gas density clearly show that there are important qualitative differences in the way Diesel sprays evolve close to the nozzle outlet. The evaluation techniques chosen for this paper highlight these differences and separate between effects due to axial and transverse spray motion.

The x-ray radiography data was supplemented with a very extensive set of optical spray images. The comparison of the two datasets indicates that important trends, such as spray penetration (not discussed in this paper due to space constraints) and spray width can be assessed using either technique. However, the absolute values obtained differ, since they are derived from related, but not from identical spray properties. The combination of the two methods yields a much more comprehensive description of the spray structure than would be available if either one of them had been used exclusively.

Acknowledgememts

This research was performed at the 1-BM-C beamline of the Advanced Photon Source, Argonne National Laboratory. This work and the use of the APS are supported by the U. S. Department of Energy under Contract No. DE-AC02-06CH11357 and by the DoE Vehicle Technologies Program, with Gurpreet Singh as a team leader.

References

1. Bittlinger, G., et al., *6th Congress on Engine Comb. Proc. and Modern Techniques*, pp. 19-30, Munich, 2003
2. Smallwood, G.J. and Gülder, Ö.L., *Atomization and Sprays*, 10:355-386, 2000
3. MacPhee, A.G., et al., *Science*, 295:1261-1263, 2002
4. Powell, C.F., et al., *Proc. 16th ILASS Americas*, Paper VIIIB.3, Monterey, CA, 2003
5. Ciatti, S., et al., *Proc. CIMAC Congress*, Paper 264, Tokyo, 2004
6. Kastengren, A.L., et al., *SAE Paper 01-0666*, 2007
7. Leick, P., et al., *21st ILASS Europe*, p. 4, Muğla, Turkey, 2007
8. Leick, P., PhD thesis, TU Darmstadt, 2008
9. Ramírez, A.I., et al., *21st ILASS Americas*, Paper W1-A-2, Orlando, FL, 2008
10. Winter, J., et al., *Proc. THIESEL Conference*, Paper A.1.3, Valencia, 2004
11. Kastengren, A.L., et al., *21st ILASS Americas*, Paper T2-B-2, Orlando, FL, 2008
12. Bittlinger, G., et al., *5th Conference on Diesel and Gasoline Direct Injection*, pp. 101-114, Berlin, 2006
13. Araneo, L., et al., *SAE Paper 01-0525*, 1999